Ionization from image states around nanotubes

G. A. Bocan,* N. R. Arista, J. L. Gervasoni,† and S. Segui†
Centro Atómico Bariloche, Comisión Nacional de Energía Atómica, Avenida Bustillo 9500, 8400 S.C. de Bariloche, Río Negro, Argentina
(Received 2 November 2007; published 31 January 2008)

We present a theoretical approach to the subject of ionization of electrons occupying an image state around a metallic nanotube. Making use of the image-electron wave function as presented by Granger *et al.* [Phys. Rev. Lett. **89**, 135506 (2002)] and performing a first order Born approximation for the transition matrix, we obtain ionization cross sections. The results show unique features which provide some hints to detect and characterize these states. A variety of situations is considered including different projectile velocities, ejection directions, and angular momenta of the image state. Both differential and total cross sections are portrayed and analyzed. The energy spectra at fixed solid angle present a double-peak structure which is a signature of the nonzero angular momentum of the image state. In addition, huge values for the total ionization cross section are predicted.

DOI: 10.1103/PhysRevB.77.035438 PACS number(s): 61.46.Fg, 34.50.−s

I. INTRODUCTION

Weakly bound electronic states with relatively long lifetimes are found in many systems, from Rydberg atoms and molecules[1–6] to nanowires,[7,8] conductor surfaces, and dielectrics.[9–17] For the case of extended structures, such as metallic surfaces of some kind, these states occur when an external electron locally polarizes the surface and becomes attracted to its image charge, residing below it. The unique properties of these image potential states (or "image states"), determined by the extreme sensitivity of image electrons to any changes in the dielectric susceptibility at the surface, make them a powerful tool for probing a variety of physical and chemical phenomena on the nanometer scale.[18–28]

Recent advances in the fabrication of nanostructured materials have enabled the exploration of these states in different nanoscopic settings such as molecular nanowires[7,8] and liquid He (Refs. 29–31) and, in a recent article, Granger *et al.*[32] have predicted image states to exist around the surfaces of freely suspended metallic nanotubes. As these tubular image states can be prepared with *nonzero angular momentum*, the resulting centrifugal barrier prevents the electrons from collapsing into the surface of the tube, thereby substantially increasing their lifetimes at low temperatures, when compared to the ones in planar systems such as graphite.[33] Also, in sharp contrast to image states above planar surfaces, the ones around a nanotube can always be localized and, hence, experimentally detectable.

Experimental evidence of image states existence around multiwalled carbon nanotubes (MWNTs) was recently provided by Zamkov *et al.*[34,35] who measured their binding energies and followed their temporal evolution by means of femtosecond time-resolved photoemission. The use of multiwalled nanotubes instead of single-walled ones (SWNT) is due to the tendency of the latter to form bundles[36] in contrast to the MWNTs which constitute an experimentally viable alternative, yielding large quantities of isolated tubes. The observation of image states in suspended SWNT networks[37] seems to be the future perspective; nevertheless, note that the potential on the vacuum side of a MWNT will have the same analytic form as that of a SWNT and therefore, theoretical predictions on SWNT could be contrasted to MWNT experimental data.

The use of narrowly focused beams, as in high resolution transmission electron microscopy,[38] provides a powerful tool for locally characterizing and analyzing nanostructure properties. In this context, we propose ionizing collisions between projectile electrons and image-state electrons around nanotubes as a way to detect the latter and gain more insight on this very active field of research.

In the article by Granger *et al.*, an approximate expression for the nanotube-image-electron potential is used in order to solve the Schrödinger equation. Starting from the image electron's wave functions and energies as given by them, in the present work, we proceed to obtain the transition matrix corresponding to the ionization of an image state by electron impact. Differential cross sections for different projectile velocities, ejection directions, and initial angular momenta of the image electron are obtained and discussed. Furthermore, some signatures of image-electron ionization are depicted in the differential and total cross sections which may be helpful in order to detect and describe such states.

II. THEORY

We consider the system wave function as given by

$$|I(F)\rangle = \frac{e^{i\bar{k}_{1i(f)}\bar{r}_1}}{(2\pi)^{3/2}}\Psi_{i(f)}(\bar{r}_2), \tag{1}$$

with $\bar{r}_1$ and $\bar{r}_2$, respectively, the space coordinate of the projectile and the target. Within a first order Born calculation, the transition matrix reads

$$T = \langle F|V|I\rangle = \frac{\tilde{V}(\bar{p})}{(2\pi)^{3/2}}\int \Psi_f^*(\bar{r}_2)e^{i\bar{p}\cdot\bar{r}_2}\Psi_i(\bar{r}_2)d\bar{r}_2, \tag{2}$$

with $\tilde{V}(\bar{p}) = 4\pi/(p^2(2\pi)^{3/2})$ the Fourier transform of the Coulombian projectile-target interaction and $\bar{p} \equiv \bar{k}_{1i} - \bar{k}_{1f}$ the momentum lost by the projectile.

Now, the target's initial state $\Psi_i(\bar{r}_2)$ is a tubular image state around a nanotube, as obtained by Granger *et al.*[32] It reads

$$\Psi_i(\bar{r}_2) = \Psi_{n,l,k_z}(\rho,\varphi,z) = \psi_{n,l}(\rho)e^{il\varphi}\frac{\phi_{k_z}(z)}{\sqrt{2\pi\rho}}, \tag{3}$$

where $\hat{z}$ is the nanotube axis and $\phi_{k_z}(z)$ will be described by means of a properly normalized Gaussian bell centered at $z=0$ with standard deviation $\sigma=100$ a.u.; regarding the target's final state $\Psi_f(\bar{r}_2)$, as a first approach, it can be described as that of a free particle, with a plane wave (PW) of momentum $\bar{k}_{2f}$. Including this information in Eq. (2) and performing the z integration, one gets

$$T^{PW} = \frac{\tilde{V}(\bar{p})}{(2\pi)^{3/2}}e^{-g_z^2\sigma^2}\sqrt{\sigma}\left(\frac{2}{\pi}\right)^{1/4} \times \int \frac{\psi_{n,l}(\rho)}{\sqrt{2\pi\rho}}\rho\left[\frac{1}{2\pi}\int_{-\pi}^{\pi} e^{ig_\parallel\rho\cos(\alpha)}e^{il\varphi}d\varphi\right]d\rho, \tag{4}$$

with $\bar{g}\equiv\bar{p}-\bar{k}_{2f}$, $\bar{g}_\parallel$ the projection of $\bar{g}$ on the x-y plane (normal to the nanotube's axis), and α the angle between $\bar{g}_\parallel$ and $\bar{\rho}$.

Choosing the x axis to be parallel to the projectile's initial velocity ($\bar{v}_{1i}=v_{1i}\hat{x}$), one finds that $\alpha=\varphi-\beta$, with β a constant for given $\bar{g}_\parallel$. Besides, in the φ integral, one can make use of the Jacobi-Anger identity[39] which reads

$$e^{iz\cos(\alpha)} = \sum_{n=-\infty}^{+\infty} i^n J_n(z)e^{in\alpha}, \tag{5}$$

and obtain

$$T^{PW} = \frac{\tilde{V}(\bar{p})}{(2\pi)^{3/2}}\sqrt{\sigma}\left(\frac{2}{\pi}\right)^{1/4}e^{il(\beta-\pi/2)} \times(-1)^l e^{-g_z^2\sigma^2}\underbrace{\int \frac{\psi_{n,l}(\rho)}{\sqrt{2\pi\rho}}\rho J_l(g_\parallel\rho)d\rho}_{I_1(g_\parallel)}. \tag{6}$$

Unfortunately, the plane wave model is not an appropriate approximation for the ionized-electron state. Given the plane wave's overlap with the initial bound state, this approach is not likely to provide accurate results in the low-energy region, as it was shown in previous studies for atomic systems.[40,41] Therefore, we choose instead to model the final ionized state by means of an orthogonalized plane wave (OPW). In this improved approach, the plane wave function of the ejected electron is orthogonalized with respect to its initial bound state, that is,

$$|OPW\rangle = |PW\rangle - \langle\psi_i|PW\rangle|\psi_i\rangle, \tag{7}$$

and the expression for the transition matrix becomes

$$T^{OPW} = T^{PW} - \frac{\tilde{V}(\bar{p})}{(2\pi)^{3/2}}\sqrt{\sigma}\left(\frac{2}{\pi}\right)^{1/4}e^{il(\beta-\pi/2)}e^{-p_z^2\sigma^2/2} \times\underbrace{\int |\psi_{n,l}(\rho_2)|^2 J_0(p_\parallel\rho_2)d\rho_2\, e^{-k_{2zf}^2\sigma^2}}_{I_2(p_\parallel)} I_1(k_{2f\parallel}), \tag{8}$$

TABLE I. Values of the parameters used in the gamma distribution to approximately reproduce $\psi_{n,l}(\rho)$ as given by Granger *et al.* (Ref. 32) for $l=6$ and $l=8$.

	$l=6$	$l=8$
ρ_0 (a.u.)	135	370
Maximum height (a.u.)	0.07	0.05
width (a.u.)	570	1000
α	5	8
β (a.u.)	35	50

where T^{PW} is given by Eq. (6). The ρ part of the target initial wave function $\psi_{n,l}(\rho)$, needed to numerically evaluate the ρ integrals in Eqs. (6) and (8), was obtained by Granger *et al.*[32] In this work, the curves portrayed in Fig. 3 of their article are fitted by gamma distributions in order to correctly reproduce the maximum's location and height, as well as the curve's width. The expression for $\psi_{n,l}(\rho)$ is

$$\psi_{n,l}(\rho) = \sqrt{\rho^{\alpha-1}\frac{e^{-\rho/\beta}}{\beta^\alpha\Gamma(\alpha)}}, \tag{9}$$

where the values of the relevant parameters are displayed in Table I.

The differential cross section for the ionization of an electron in state $\{n,l\}$ is easily expressed in terms of the transition matrix and reads

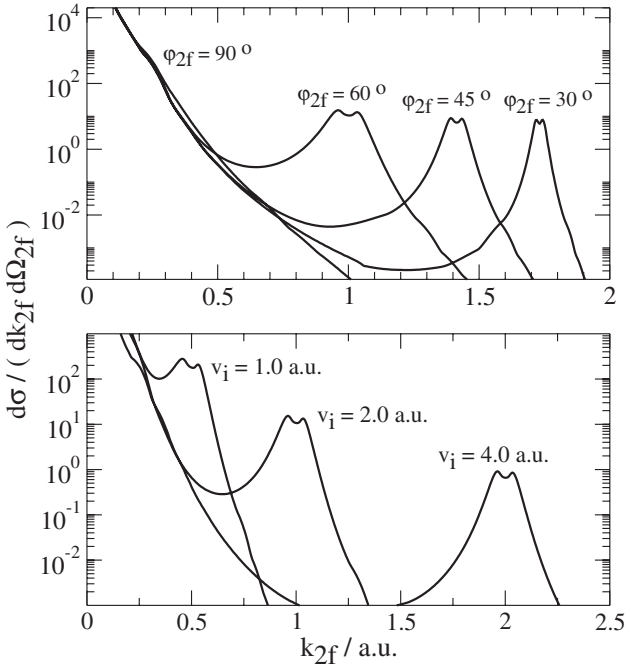

FIG. 1. Differential cross sections for the ionization of an electron bound to the nanotube in the image state corresponding to $n=1$, $l=6$. Momentum spectra are displayed for the plane perpendicular to the nanotube ($\theta_{2f}=90°$). (a) $v_i=2.0$ a.u. and different angles with respect to the projectile's initial velocity. (b) $\varphi_{2f}=60°$ and different projectile velocities.

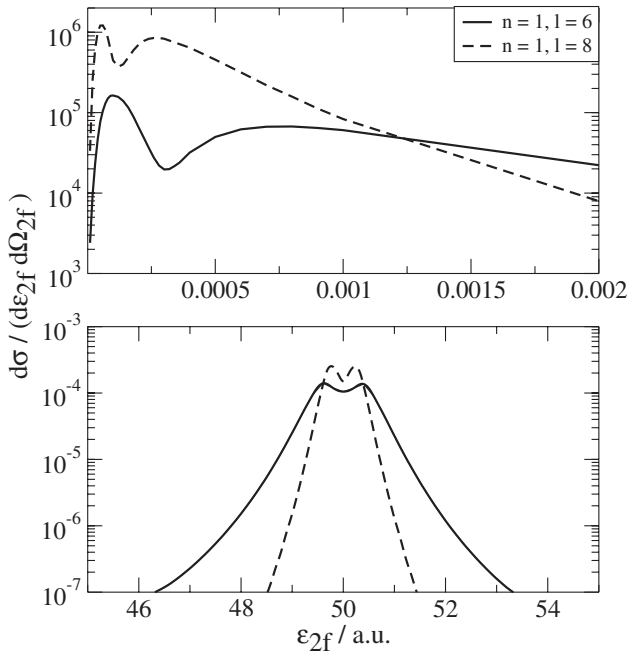

FIG. 2. Differential cross section for image-electron ionization. The projectile velocity v_i=20 a.u. and the ejection direction considered is θ_{2f}=90°, φ_{2f}=60°. Top: low-energy region. Bottom: double-peak region.

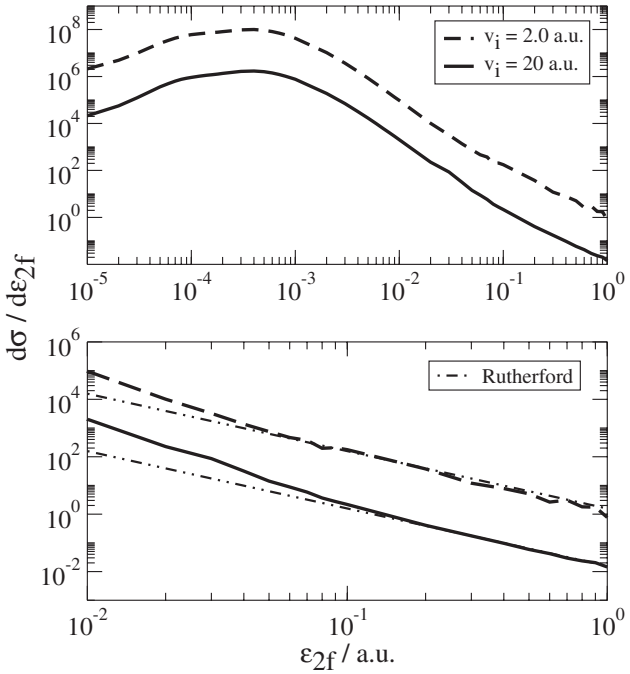

FIG. 3. Differential cross section with integrated ejection solid angle. The image state is n=1, l=6. Top: results for v_i=2.0 a.u. and v_i=20.0 a.u. Bottom: detail of the intermediate to high-energy regime. Results for Rutherford scattering are displayed as well for both velocities.

$$d\sigma_{n,l} = \frac{(2\pi)^3}{v_i} 2\pi\delta(E_i - E_f)|T|^2 d\bar{p} d\bar{k}_{2f}, \tag{10}$$

with E_i, E_f the system's initial and final energies. In this paper, the image states {1,6} and {1,8} will be considered, with corresponding binding energies $\varepsilon_{1,6}$=0.000 44 a.u. and $\varepsilon_{1,8}$ =0.000 15 a.u.[32]

III. RESULTS

In Fig. 1, the differential cross section is displayed as a function of the ionized-electron momentum for fixed solid angle $d\Omega_{2f}=\sin(\theta_{2f})d\theta_{2f}d\varphi_{2f}$ and projectile velocity. The image state considered is the one with quantum numbers n=1, l=6, which, according to Granger *et al.*,[32] is the minimum l value that supports image states. In Fig. 1(a), results are portrayed for a projectile velocity v_i=2.0 a.u. and a variety of ionization directions, all contained in the plane perpendicular to the nanotube's axis and measured with respect to the projectile's initial direction ($\hat{x}$). In Fig. 1(b), a direction is chosen and differential cross sections are displayed for various projectile velocities. The characteristics observed in these graphs can be explained by means of the energy and momentum conservation equations for a nearly free particle, given the fact that the binding energy for the image electron is almost negligible. The cross section presents what appears to be a divergence for $k_{2f}\rightarrow 0$ (in Fig. 2, we will see that it is not) and a clear double-peak structure centered at the binary peak position $[k_{2f}=v_i\cos(\varphi_{2f})]$ which is easily understood within a semiclassical representation as due to the nonzero initial angular momentum of the image electron.

Moving now to higher projectile velocities, in Fig. 2, differential cross sections are plotted for v_i=20 a.u.. in the direction θ_{2f}=90°, φ_{2f}=60°. Two different image states are considered, and for both, one finds two distinct structures. On the one hand, the double peak already discussed (bottom figure) and, on the other (top figure), a huge structure at a very low energy of the order of the binding energy, whose position is determined solely by it, and which takes the place of the zero-energy divergence expected for free particle Coulomb scattering.

In Fig. 3, differential cross sections are shown as a function of the ejected-electron energy, integrated in solid angle (first differential energy spectra). The state under consideration is again n=1, l=6, and results for two projectile velocities are displayed. It is interesting to observe that, based on the top figure, one can assure that the total cross section will be almost purely determined by the low-energy structure contribution. As for the bottom figure, it displays the detail of the intermediate to high-energy region where the Rutherford limit is correctly reached.

Next, in Fig. 4, the total cross sections are displayed as a function of the projectile initial velocity for image states {1,6} and {1,8}. Results obtained for the PW model are depicted as well, for comparison. It is observed that both models present an abrupt threshold at a projectile velocity corresponding to the binding energy. However, while the PW results rapidly saturate becoming v_i independent, the OPW calculations display a more realistic decreasing behavior at high impact energies, which qualitatively resembles the one found in ionization of H^{40} and H^{-41}, despite the much larger binding energies for these latter systems.

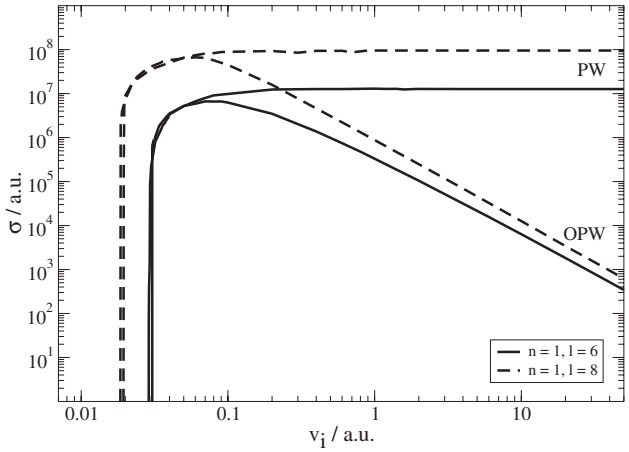

FIG. 4. Total cross sections as a function of the projectile initial velocity. Results are displayed for image states {1,6} and {1,8}. Although results for $v_i < 1$ a.u. are below the Born approximation validity range; they have been added to the graph in order to show the threshold existence.

Finally, it is worth remarking on the extremely high values obtained for the cross sections of image-state ionization. Their magnitude is due not only to these states, large geometrical area, but also to their very weak binding. The result is thus a process with a very large occurrence probability and therefore highly significant to experimental spectral analysis.

IV. SUMMARY

In summary, the problem of image-electron ionization has been theoretically addressed and the corresponding differential cross sections have been presented for a variety of projectile velocities, ejection directions, and initial angular momenta of the image state. A double-peak structure has been found in the differential energy spectra, which is explained as a consequence of the nonzero initial angular momentum of the electron to be ionized; besides, a very high-low-energy structure has been observed, whose position is determined by the small binding energy.

In the light of the current interest for the properties of nanotubes, image states, and related phenomena, there is much profit to be obtained from the comparison of our results and conclusions with experimental data. The double-peak structure presented in this paper could eventually be found in spectroscopy studies using charged particle beams, providing an independent test of existence for tubular image states around nanotubes. However, to our knowledge, those experimental data are presently unavailable.

ACKNOWLEDGMENTS

The authors are grateful to M. S. Moreno and J. E. Miraglia for several useful discussions. This work was made thanks to the financial support of the ANPCyT, PICT-R 122/02.

*Present address: Donostia International Physics Center, Paseo Manuel de Lardizabal 4, 20018, Donostia-San Sebastián, Spain.
†Also at Consejo Nacional de Investigaciones Científicas y Técnicas (CONICET) Argentina.

[1] T. Gallagher, *Rydberg Atoms* (Cambridge University Press, New York, 1994).
[2] T. C. Killian, M. J. Lim, S. Kulin, R. Dumke, S. D. Bergeson, and S. L. Rolston, Phys. Rev. Lett. **86**, 3759 (2001).
[3] W. R. Anderson, J. R. Veale, and T. F. Gallagher, Phys. Rev. Lett. **80**, 249 (1998).
[4] W. G. Scherzer, H. L. Selzle, E. W. Schlag, and R. D. Levine, Phys. Rev. Lett. **72**, 1435 (1994).
[5] C. H. Greene, A. S. Dickinson, and H. R. Sadeghpour, Phys. Rev. Lett. **85**, 2458 (2000).
[6] B. E. Granger, E. L. Hamilton, and C. H. Greene, Phys. Rev. A **64**, 042508 (2001).
[7] J. E. Ortega, F. J. Himpsel, R. Haight, and D. R. Peale, Phys. Rev. B **49**, 13859 (1994).
[8] I. G. Hill and A. B. McLean, Phys. Rev. Lett. **82**, 2155 (1999).
[9] N. D. Lang and W. Kohn, Phys. Rev. B **7**, 3541 (1973).
[10] P. M. Echenique and J. B. Pendry, J. Phys. C **11**, 2065 (1978).
[11] R. Shakeshaft and L. Spruch, Phys. Rev. A **31**, 1535 (1985).
[12] P. M. Echenique, F. Flores, and F. Sols, Phys. Rev. Lett. **55**, 2348 (1985).
[13] E. V. Chulkov, I. Sarría, V. M. Silkin, J. M. Pitarke, and P. M. Echenique, Phys. Rev. Lett. **80**, 4947 (1998).
[14] S. Schuppler, N. Fischer, Th. Fauster, and W. Steinmann, Phys. Rev. B **46**, 13539 (1992).
[15] J. Osma, I. Sarría, E. V. Chulkov, J. M. Pitarke, and P. M. Echenique, Phys. Rev. B **59**, 10591 (1999).
[16] M. Wolf, E. Knoesel, and T. Hertel, Phys. Rev. B **54**, R5295 (1996).
[17] D. Straub and F. J. Himpsel, Phys. Rev. B **33**, 2256 (1986).
[18] M. Machado, W. Berthold, U. Höfer, E. V. Chulkov, and P. M. Echenique, Science **277**, 1480 (1997).
[19] T. Hertel, E. Knoesel, M. Wolf, and G. Ertl, Phys. Rev. Lett. **76**, 535 (1996).
[20] A. D. Miller, I. Bezel, K. J. Gaffney, S. Garrett-Roe, S. H. Liu, P. Szymanski, and C. B. Harris, Science **297**, 1163 (2002).
[21] W. Berthold, U. Höfer, P. Feulner, E. V. Chulkov, V. M. Silkin, and P. M. Echenique, Phys. Rev. Lett. **88**, 056805 (2002).
[22] D. C. Marinica, C. Ramseyer, A. G. Borisov, D. Teillet-Billy, J. P. Gauyacq, W. Berthold, P. Feulner, and U. Höfer, Phys. Rev. Lett. **89**, 046802 (2002).
[23] D. F. Padowitz, W. R. Merry, R. E. Jordan, and C. B. Harris, Phys. Rev. Lett. **69**, 3583 (1992).
[24] R. L. Lingle, D. F. Padowitz, R. E. Jordan, J. D. McNeill, and C. B. Harris, Phys. Rev. Lett. **72**, 2243 (1994).
[25] T. Schmitz-Hübsch, K. Oster, J. Radnik, and K. Wandelt, Phys. Rev. Lett. **74**, 2595 (1995).
[26] P. D. Loly and J. B. Pendry, J. Phys. C **16**, 423 (1983).
[27] R. Fischer, Th. Fauster, and W. Steinmann, Phys. Rev. B **48**, 15496 (1993).
[28] N. Memmel and E. Bertel, Phys. Rev. Lett. **75**, 485 (1995).

[29] P. M. Platzman and M. I. Dykman, Science **284**, 1967 (1999).
[30] C. C. Grimes and T. R. Brown, Phys. Rev. Lett. **32**, 280 (1974).
[31] P. Glasson, V. Dotsenko, P. Fozooni, M. J. Lea, W. Bailey, G. Papageorgiou, S. E. Andresen, and A. Kristensen, Phys. Rev. Lett. **87**, 176802 (2001).
[32] B. E. Granger, P. Král, H. R. Sadeghpour, and M. Shapiro, Phys. Rev. Lett. **89**, 135506 (2002).
[33] J. Lehmann, M. Merschdorf, A. Thon, S. Voll, and W. Pfeiffer, Phys. Rev. B **60**, 17037 (1999).
[34] M. Zamkov, H. S. Chakraborty, A. Habib, N. Woody, U. Thumm, and P. Richard, Phys. Rev. B **70**, 115419 (2004).
[35] M. Zamkov, N. Woody, B. Shan, H. S. Chakraborty, Z. Chang, U. Thumm, and P. Richard, Phys. Rev. Lett. **93**, 156803 (2004).
[36] J. Liu, A. G. Rinzler, H. Dai, J. H. Hafner, R. K. Bradley, P. J. Boul, A. Lu, T. Iverson, K. Shelimov, C. B. Huffman, F. Rodriguez-Macias, Y.-S. Shon, T. R. Lee, D. T. Colbert, and R. E. Smalley, Science **280**, 1253 (1998).
[37] Y. Homma, Y. Kobayashi, T. Ogino, and T. Yamashita, Appl. Phys. Lett. **81**, 2261 (2002).
[38] Z. L. Wang, Micron **27**, 265 (1996).
[39] *Handbook of Mathematical Functions*, edited by M. Abramowitz and I. A. Stegun (Dover, New York, 1964).
[40] M. R. C. McDowell and J. P. Coleman, *Introduction to the Theory of Ion-Atom Collisions* (North-Holland, Amsterdam, 1970).
[41] D. F. Dance, M. F. A. Harrison, and R. D. Rundel, Proc. R. Soc. London **A299**, 525 (1967).